Available online at www.sciencedirect.com
ScienceDirect
Ceramics International 37 (2011) 3133–3138
CERAMICS INTERNATIONAL
www.elsevier.com/locate/ceramint

Synthesis of nanocrystalline ytterbium-doped yttria by citrate-gel combustion method and fabrication of ceramic materials

Nengli Wang *, Xiyan Zhang, Zhaohui Bai, Haiying Sun, Quansheng Liu, Liping Lu, Xiaoyun Mi, Xiaochun Wang

School of Materials Science and Engineering, Changchun University of Science and Technology, Changchun 130022, China

Received 14 February 2011; received in revised form 5 May 2011; accepted 16 May 2011
Available online 23 May 2011

Abstract

Nanosized ytterbium doped yttria powders were prepared by citrate-gel combustion techniques. As-synthesized precursor and calcined powders were characterized for their crystalline structure, particle size and morphologies. Nanocrystalline Yb^{3+}:Y_2O_3 powders with pure cubic yttria crystal structure were obtained by calcination of as-prepared precursors at 1100 °C for 3 h. Powders obtained were well dispersed with an average particle size of 60 nm. By using the obtained powders, nearly full dense Yb^{3+}:Y_2O_3 ceramics were produced by vacuum sintering at 1800 °C for 12 h. The emission spectrum of the sintered ceramics under the excitation wavelength of 905 nm illustrates that there are three fluorescence peaks locating at 976 nm, 1030 nm and 1075 nm respectively, all corresponding to the $^2F_{5/2} \rightarrow {}^2F_{7/2}$ transitions of ytterbium ion.

Keywords: A. Sol–gel processes; A. Sintering; C. Optical properties; D. Y_2O_3

1. Introduction

As an attractive laser host material for trivalent lanthanide activators, cubic yttria (Y_2O_3) crystal has been investigated for a long time because it has good thermal, mechanical, chemical and optical properties [1–5]. In particular, the thermal conductivity of Y_2O_3 is about 20–30% larger than that of $Y_3Al_5O_{12}$ (YAG) while the thermal expansion coefficients are nearly the same. However, It is difficult to grow a Y_2O_3 single crystal by any conventional growth methods because of its high melting point (~2430 °C) and the polymorphic phase from C to a high temperature hexagonal phase H at about 2350 °C [6,7]. With the development of nanocrystalline technology, it has been possible to fabricate highly transparent ceramics for solid-state lasers by a vacuum sintering technique. Polycrystalline transparent yttria ceramics is a promising substitute for single crystal yttria, because ceramic techniques has many advantages such as simplicity, ease of fabrication, and mass production in a large size [8]. Among the trivalent rare-earth ion doped yttria ceramics, ytterbium-doped yttria (Yb^{3+}:Y_2O_3) has attracted considerable attentions. Yb^{3+} ions have a very simple electronic structure with only two manifolds separated by about 10,000 cm^{-1}. So, there is no intrinsic process for concentration quenching. Owing to perceptible electron–phonon interaction, Yb^{3+} doped materials have broad absorption in near-IR which is suitable for laser diode (LD) pumping. The broad luminescence band $^2F_{5/2} \rightarrow {}^2F_{7/2}$ is also attractive for ultra-short pulse generation. Therefore, Yb^{3+}:Y_2O_3 ceramics possess great potentials as a laser media for LD-pumped solid-state lasers [6,7,9–11].

Superfine yttria nanopowders with good dispersivity and suitable particle size distribution have an important advantage for fabricating high-performance Y_2O_3 transparent ceramics. Wet-chemical routes, including sol–gel [12,13], co-precipitation [14,15] and combustion method [16–18], have been proved to be suitable for preparation of nanometer-size particles with favorable sinterability due to their characteristics of the uniform mixing of starting materials and the excellent chemical homogeneity of the final products. Among these preparation techniques, combustion method has been developed and widely used in recent years. Combustion technique is simple, inexpensive and less time consuming, it involves the

* Corresponding author. Tel.: +86 431 85583016.
E-mail address: wang_nengli@sina.com (N. Wang).

0272-8842/$36.00
doi:10.1016/j.ceramint.2011.05.053

exothermic combustion reaction between oxidant, generally metal nitrates and an organic fuel. During the combustion reaction, larger amount of gas evolves and results in a porous product which can be easily crushed and ground into fine powders. These processes yield reactive powders with high purity, fine particle size and low sintering temperature compared to the powders prepared by conventional method. The present investigation reports the synthesis of 3 at% Yb^{3+} doped Y_2O_3 nanopowders by ceramic combustion techniques using citric acid as fuels in combustion reaction. Fabrication of yttria ceramics using the synthesized Yb^{3+}:Y_2O_3 nanopowders as starting material under vacuum conditions were also performed.

2. Experimental

Citrate-gel combustion method is a modified sol–gel technique in which the gel is decomposed by a self-propagating high temperatures synthesis (SHS) process. It is a combination of sol–gel and SHS reaction processes. An aqueous nitrate solution of Y^{3+} and Yb^{3+} were prepared by dissolving Y_2O_3 (99.99%) and Yb_2O_3 (99.99%) in diluted nitric acid under stirring at 80 °C for 2 h. The metal nitrates were weighted according to the required proportion and mixed in a glass cylindrical beaker with doping of minor amount of ammonium sulfate ($(NH_4)_2SO_4$) as a dispersant. Double distilled water was used in the experiments for homogenous mixing of metal nitrates. Citric acid was added to the mixtures as a fuel and mixed thoroughly followed by a clear solution was obtained. It was calculated that 1.667 mol of citric acid was required to prepare 1 mol of yttria with complete combustion. The equivalence ratio, i.e., the ratio of the oxidizing valency to reducing valency (O/F) was maintained at unity (O/F = 1). The valency of nitrogen was not considered because of its conversion to molecular nitrogen (N_2) during combustion. The assumed complete combustion reactions can be written as:

$$6Re(NO_3)_3 + 5CH_2COOHCOHCOOHCH_2COOH = 3Re_2O_3 + 9N_2\uparrow + 30CO_2\uparrow + 20H_2O\uparrow$$

The mixed solution in the glass beaker was kept in a water-bath of 80 °C for 8 h until it transformed into a honey-like yellow transparent gel. The gel was dried at 120 °C for 24 h and became a deep-yellow sticky gel. This gel was rapidly heated to 300 °C and at this stage an auto combustion process occurred accompanied with a brown fume, and finally yielded a fluffy precursor. The precursor was crushed and then heat treated at temperatures ranging from 600 °C to 1100 °C for 3 h in an oxygen atmosphere. For sintering, powders calcined at 1100 °C for 3 h were dry pressed into Ø 15 mm pellets in a steel mold at 30 MPa and then cold isostatically pressed (CIP) at 200 MPa. The pellets were then sintered under vacuum at 1800 °C. The vacuum in the furnace was 10^{-3} Pa during the sintering period.

Phase composition of the samples was identified by X-ray diffraction (XRD, Model D/Max-rA, Rigaku, Japan) with a CuKα radiation source (λ = 0.15406 nm). Fourier transform infrared spectroscopy (FTIR) of the samples was measured on a Shimadzu FTIR-8400S spectrometer in the range of 4000–400 cm^{-1} using the standard KBr method. The morphology of powders and the microstructures of sintered ceramics were analyzed by high resolution cold FEG scanning electron microscope (FE-SEM, Model JSM-6701F, Japan). Element distribution of the ceramic sample was carried out by Energy-dispersive X-ray spectroscopy (EDS, Model Oxford INCA X–Sight). The excitation and emission spectra of the ceramics were measured using a spectrofluorometer (Model Fluorolog-3, Jobin Yvon Spex) at room temperature.

3. Results and discussion

3.1. X-ray diffraction

Fig. 1 shows the XRD patterns of the precursor and powders calcined at different temperatures for 3 h. It seems to be an amorphous phase in as-prepared citrate-gel precursor (Fig. 1(a)), and there is no crystalline phase observed in the XRD pattern of the precursor. Citric acid is widely used in sol–gel process to obtain amorphous polyatomic materials [19]. With the increase of calcination temperature, characteristic peaks of yttria phase start to appear with rather weak intensity, indicating crystallization of the amorphous powder. All the characteristic XRD peaks of yttria appear when calcined at 700 °C, and the diffraction peaks agree well with that of Y_2O_3

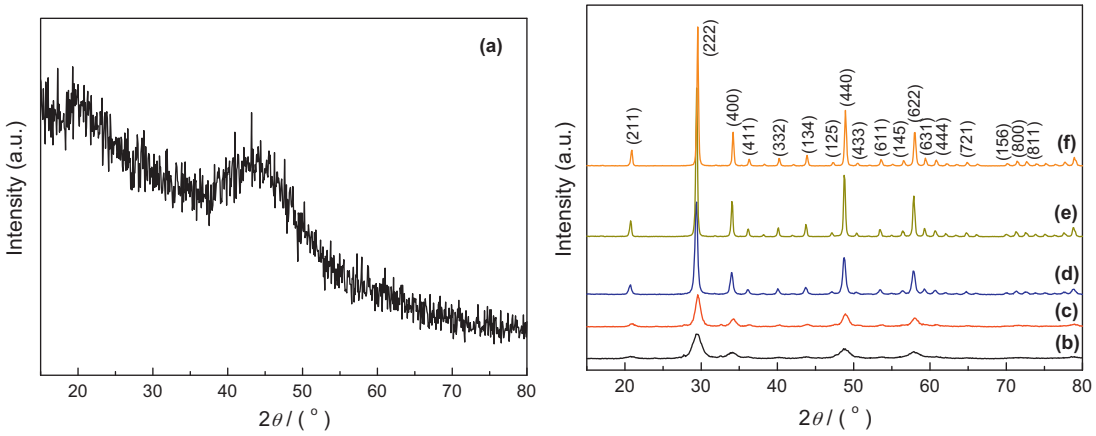

Fig. 1. XRD patterns of (a) citrate-gel precursor and powders calcined at (b) 600 °C, (c) 700 °C, (d) 800 °C, (e) 1000 °C and (f) 1100 °C for 3 h.

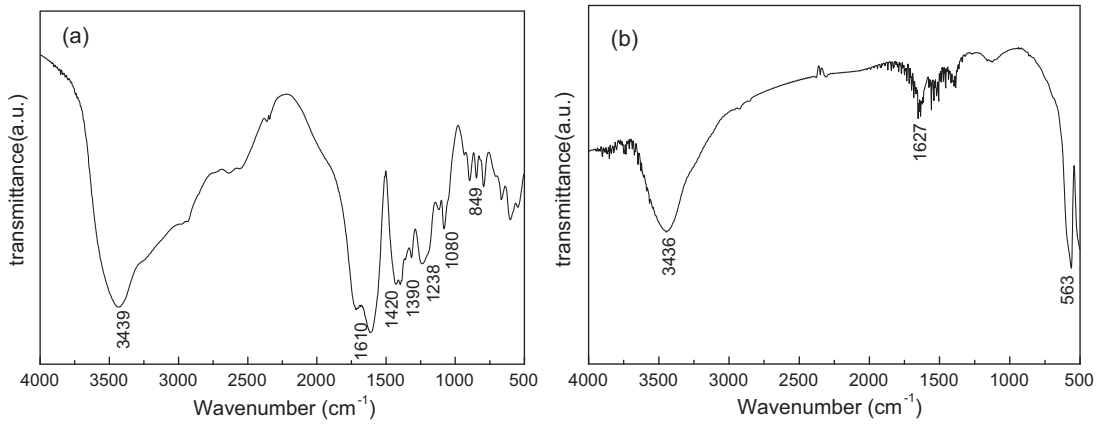

Fig. 2. FTIR spectra of (a) citrate gel precursor and (b) powder calcined at 1100 °C for 3 h.

crystal structure (JCPDS Card No. 83-0927). The diffraction peaks of Y_2O_3 phase become much sharper with the increase of calcination temperature, indicating the continuation of the crystallization process. The crystal growth of Y_2O_3 phase is responsible for this phenomenon. No secondary phases are detected, indicating that in the case of Yb-doped yttria powders, they form a solid solution by substitutioning Y with Yb in the Y_2O_3 lattice.

3.2. Infrared spectra analysis

The FTIR spectra of the citrate-gel precursor and powder calcined at 1100 °C for 3 h are shown in Fig. 2. In Fig. 2(a), the absorption peaks centered at 3439 cm^{-1} and 1610 cm^{-1} should be attributed to O–H stretching and bending vibrations respectively. Since the starting materials contained significant amounts of hydroxyl groups, their absorption bands in the FTIR spectra are expected. Presence of carboxylate anion –COO– group is confirmed by bands at 1420 and 1390 cm^{-1} which correspond to symmetrical vibrations of –COO– group, and band at 1238 cm^{-1} can be attributed to the C–O stretching vibration in carboxylate. Bands locate at 1080 cm^{-1} and 849 cm^{-1} corresponds to the presence of CO_3^{2-} and NO_3^- respectively. Fig. 2(a) indicates that the combustion process of the gel precursor is incomplete. After calcining at 1100 °C for 3 h, the absorption peaks from organic carboxylate composition disappear, which can be seen from Fig. 2(b). There are also no evidences of residual CO_3^{2-} and NO_3^- can be found in Fig. 2(b), the weak peaks observed at 3436 and 1627 cm^{-1} are assigned to –OH group of water or moisture present on the surface of the powders, the peaks obtained below 580 cm^{-1} are attributed to the metal–oxide (Y–O) vibration bands, indicating the complete crystallization of Y_2O_3. It can be seen that the FTIR analysis is in accordance with the XRD results.

3.3. Morphology characterization of the calcined powders

Fig. 3 shows SEM morphologies of the Yb^{3+}:Y_2O_3 nanopowders calcined at 1100 °C for 3 h with out (Fig. 3(a)) and with (Fig. 3(b)) ammonium sulfate doping. From Fig. 3(b), it can be seen that particles with sulfate doping disperse uniformly, and have a relatively narrow size distribution. Most particles are spherical in shape with the average particle size of about 60 nm. The release of gas in the combustion process gave a significantly porous structure in the calcined powders, and this is beneficial to the dispersion of powders. Compared with Fig. 3(b), powder without sulfate doping has a lower dispersivity and a wide size distribution with a range from

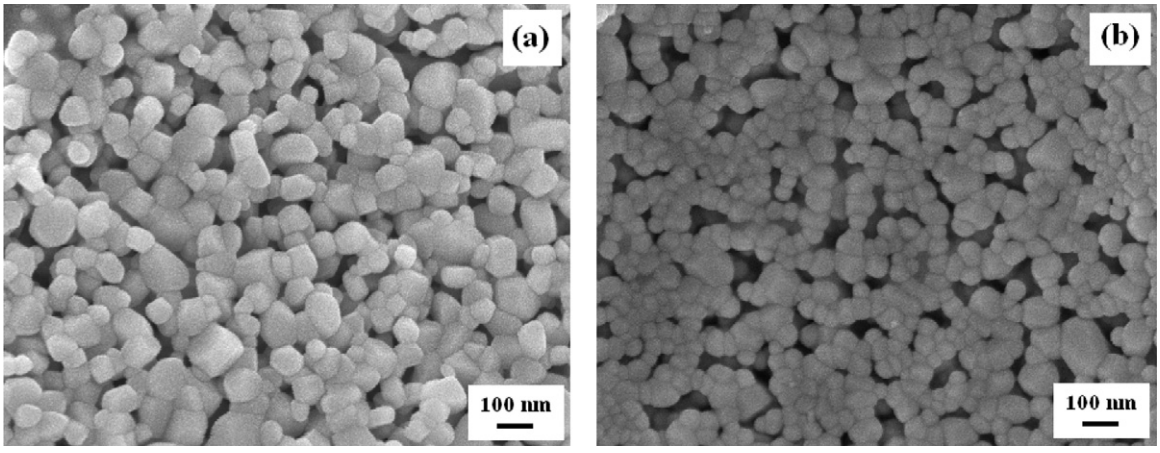

Fig. 3. SEM morphologies of Yb^{3+}:Y_2O_3 powders calcined at 1100 °C without sulfate ions doping (a) and doped with sulfate ions (b).

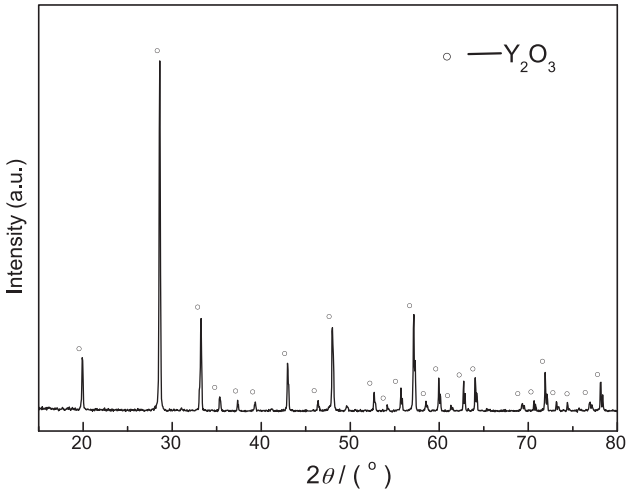

Fig. 4. XRD patterns of Yb^{3+}:Y_2O_3 ceramics sintered at 1800 °C for 12 h.

50 nm to 90 nm, and is not so uniform with a mixture of spherical and rectangular in morphology.

According to Wen et al. [15,20], the precursor has a positive ζ potential in aqueous solution, hence SO_4^{2-} can be absorbed onto the surface of the precursor particles due to the electrostatic force. The SO_4^{2-} has a higher decomposition temperature and its existence at comparatively high temperature may reduce the element diffusion between particles, resulting in a smaller particle size. Its decomposition at higher temperatures is also beneficial for the dispersion of powder during calcination. Powders with such qualities have high sinterability to the fabrication of transparent yttria ceramics [15,20,21].

3.4. Microstructure and spectroscopic properties of sintered Yb^{3+}:Y_2O_3 ceramics

Fig. 4 shows the XRD pattern of Yb^{3+}:Y_2O_3 ceramics sintered at 1800 °C for 12 h under vacuum. The sample is well crystallized and exhibits a pure cubic phase of Y_2O_3 structure without the presence of Yb_2O_3 phase or other impurities.

Fig. 5 is the SEM images of fracture surfaces of the sintered yttria ceramic samples by vaccum sintering process under

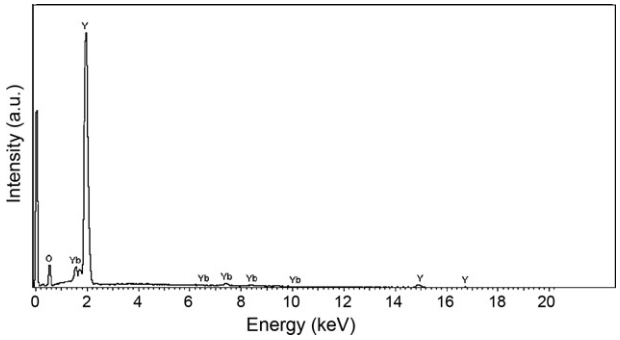

Fig. 6. EDS mapping spectrum of 3 at% Yb^{3+}:Y_2O_3 ceramics.

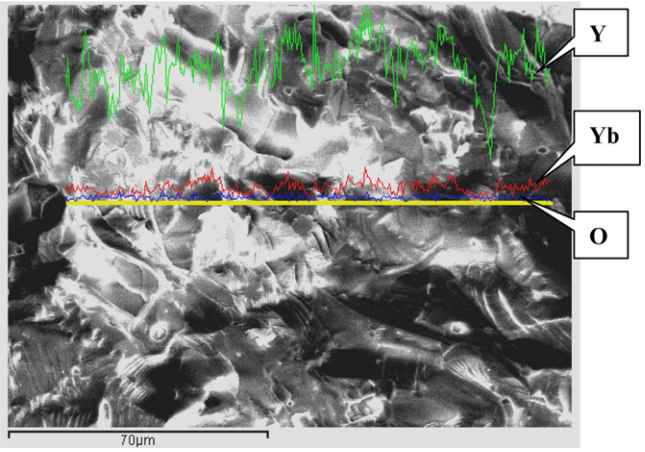

Fig. 7. EDS line scan spectrum of 3 at% Yb^{3+}:Y_2O_3 ceramics.

1800 °C for 5 h (Fig. 5(a)) and for 12 h (Fig. 5(b)). The presence of a great number of porosity at grain boundary junctions and as clusters in the grain interior can be seen in the sample sintered for 5 h. With the increase of sintering time, a significant grain growth and densification has occurred in the sample, it can be seen that nearly pore-free microstructure of the sample remained homogeneous without abnormal grain growth, and transgranular fracture indicates that no pore entrapment has occurred in the densified regions (Fig. 5(b)). The corresponding energy dispersive X-ray spectrometry (EDS) mapping spectrum of the ceramic sample sintered for

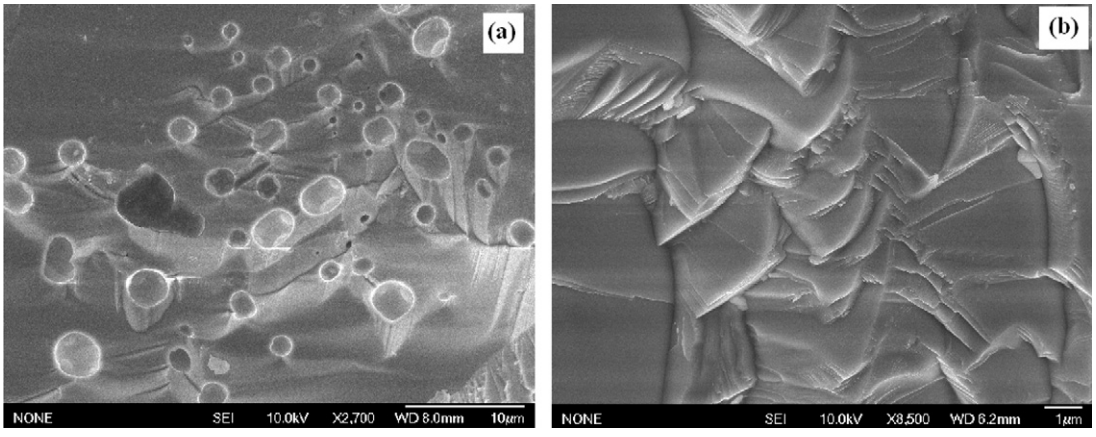

Fig. 5. Fracture surface for Yb^{3+}:Y_2O_3 ceramics sintered at 1800 °C for: (a) 5 h and (b) 12 h.

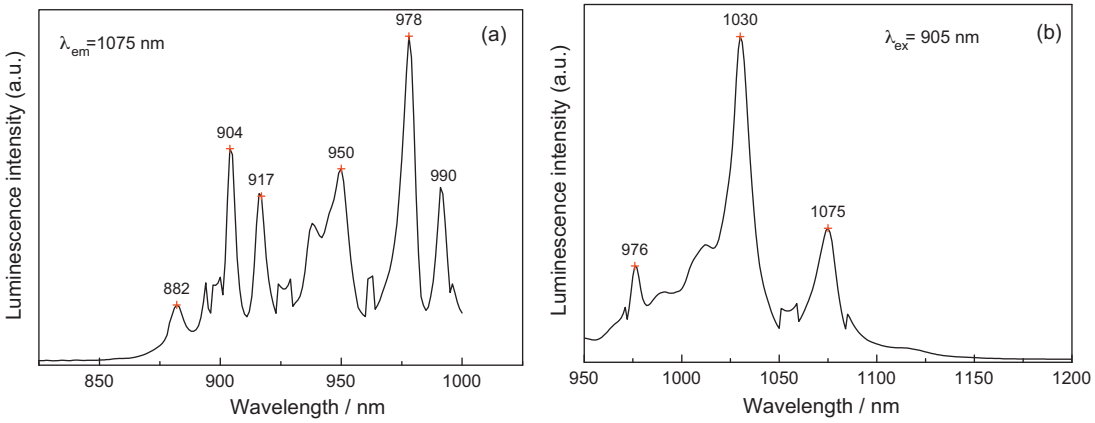

Fig. 8. Excitation (a) and emission (b) spectra of sintered Yb^{3+}:Y_2O_3 ceramics.

12 h (Fig. 6) was taken and the elemental signatures of Y, Yb, and O are essentially identical within experimental accuracy. Fig. 7 shows the EDS line scan spectrum of the same ceramic sample, it can be seen that Yb element (blue-colour line) is equally distributed both in grains and grain boundaries, indicating a homogeneous doping of ytterbium element. Using vacuum sintering at higher temperatures (usually >1700 °C), transparent Yb^{3+}:Y_2O_3 ceramics is supposed to be fabricated by eliminating the pores between the grain boundaries, which is under investigation by our laboratory.

The optical spectra of Yb^{3+}:Y_2O_3 ceramics sintered at 1800 °C for 12 h are shown in Fig. 8. The excitation spectrum of the sample (Fig. 8(a)) with the monitoring wavelength of 1075 nm consists of a series of peaks ranging from 880 nm to 1000 nm. The broad absorption bands of Yb^{3+}:Y_2O_3 ceramics in 900–1000 nm make it suitable to be coupled by laser diode, hence the temperature control of LD is unnecessary [22]. Fig. 8(b) is the emission spectrum of the ceramic sample (λ_{ex} = 905 nm). There are three main emission peaks, which centered at 976 nm, 1030 nm and 1075 nm respectively, all corresponding to the transitions from the sublevels of $^2F_{5/2}$ to the components of the ground state of $^2F_{7/2}$. The spectra analysis results obtained are in accordance with those reported earlier in Refs. [6,9,22].

4. Conclusions

Nanocrystalline yttria powders doped with 3 at% of ytterbium were synthesized by a citrate-gel combustion method with $(NH_4)_2SO_4$ as a dispersant. The single phase crystalline yttria powders have been obtained when calcined at 700 °C. Powder calcined at 1100 °C has a spherical morphology and homogeneously dispersed with an average particle size of 60 nm. Nearly fully dense Yb^{3+}:Y_2O_3 ceramics have been fabricated from the powders calcined at 1100 °C by vacuum sintering at 1800 °C for 12 h and exhibited a homogenous microstructure.

References

[1] N.S. Prasad, W.C. Edwards, S.B. Trivedi, S.W. Kutcher, C.C. Wang, J.S. Kim, U. Hömmerich, V. Shukla, R. Sadangi, B.H. Kear, Recent progress in the development of neodymium-doped ceramic yttria, IEEE Journal of Selected Topics in Quantum Electronics 13 (3) (2007) 831–837.
[2] V. Lupei, Comparative spectroscopic investigation of rare earth-doped oxide transparent ceramics and single crystals, Journal of Alloys and Compounds 451 (2008) 52–55.
[3] V. Lupei, A. Lupei, A. Ikesue, Single crystal and transparent ceramic Nd-doped oxide laser materials: a comparative spectroscopic investigation, Journal of Alloys and Compounds 380 (2004) 61–70.
[4] H. Eilers, Fabrication, optical transmittance, and hardness of IR-transparent ceramics made from nanophase yttria, Journal of the European Ceramic Society 27 (2007) 4711–4717.
[5] X Hou, S. Zhou, H. Lin, H. Teng, Y. Li, W. Li, T. Jia, Violet and blue upconversion luminescence in Tm^{3+}/Yb^{3+} codoped Y_2O_3 transparent ceramic, Journal of Applied Physics 107 (2010) 083101.
[6] J. Kong, D.Y. Tang, B. Zhao, J. Lu, K. Ueda, H. Yagi, T. Yanagitani, 9.2-W diode-end-pumped Yb:Y_2O_3 ceramic laser, Applied Physics Letters 86 (2005) 161116–161121.
[7] H.X. Ma, Q.H. Liu, Y.F. Qi, J.X. Dong, Y.R. Wei, 5.5 W CW Yb^{3+}:Y_2O_3 ceramic laser pumped with 970 nm laser diode, Optics Communications 246 (2005) 465–469.
[8] G.A. Kumar, J. Lu, A.A. Kaminskii, K.I. Ueda, H. Yagi, T. Yanagitani, Spectroscopic and stimulated emission characteristics of Nd^{3+} in transparent Y_2O_3 ceramics, IEEE Journal of Quantum Electronics 42 (7) (2006) 643–650.
[9] K. Takaichi, H. Yagi, J. Lu, J.F. Bission, A. Shirakawa, K.I. Ueda, T. Yanagitani, A.A. Kaminskii, Highly efficient continuous-wave operation at 1030 and 1075 nm wavelengths of LD-pumped Yb^{3+}:Y_2O_3 ceramic lasers, Applied Physics Letters 84 (2004) 317–319.
[10] G.Q. Xie, D.Y. Tang, L.M. Zhao, L.J. Qian, K. Ueda, High-power self-mode-locked Yb:Y_2O_3 ceramic laser, Optics Letters 32 (18) (2007) 2741–2743.
[11] L.D. Merkle, G.A. Newburgh, N.T. Gabrielyan, A. Michael, M. Dubinskii, Temperature-dependent lasing and spectroscopy of Yb:Y_2O_3 and Yb:Sc_2O_3, Optics Communications 281 (2008) 5855–5861.
[12] J. Zhang, Z. Zhang, Z. Tang, Y. Lin, Z. Zheng, Luminescent properties of Y_2O_3:Eu synthesized by sol–gel processing, Journal of Materials Processing Technology 121 (2002) 265–268.
[13] A. Leleckaite, A. Kareiva, H. Bettentrup, T. Jüstel, H.J. Meyer, Sol–gel preparation and characterization of codoped yttrium aluminium garnet powders, Zeitschrift fur Anorganische und Allgemeine Chemie 631 (2005) 2987–2993.
[14] S. Bhattacharyya, S. Ghatak, Synthesis and characterization of YAG precursor powder in the hydroxyhydrogel form, Ceramics International 35 (2009) 29–34.
[15] L. Wen, X. Sun, Q. Lu, G. Xu, X. Hu, Synthesis of yttria nanopowders for transparent yttria ceramics, Optical Materials 29 (2006) 239–245.
[16] R.V. Mangalaraja, J. Mouzon, P. Hedsröm, C.P. Camurri, S. Ananthakumar, M. Odén, Microwave assisted combustion synthesis of nanocrystalline yttria and its powder characteristics, Powder Technology 191 (2009) 309–314.

[17] T. Feng, J. Shi, D. Jiang, Optical properties of transparent Pr:YSAG ceramic, Ceramics International 35 (2009) 427–431.
[18] J. Mouzon, C. Dujardin, O. Tillement, M. Odén, Synthesis and optical properties of $Yb_{0.6}Y_{1.4}O_3$ transparent ceramics, Journal of Alloys and Compounds 464 (2008) 407–411.
[19] A. Dupont, C. Parent, B.Le. Garrec, J.M. Heintz, Size and morphology control of Y_2O_3 nanopowders via a sol–gel route, Journal of Solid State Chemistry 171 (2003) 152–160.
[20] L. Wen, X. Sun, Z. Xiu, S. Chen, C.T. Tsai, Synthesis of nanocrystalline yttria powder and fabrication of transparent YAG ceramics, Journal of the European Ceramic Society 24 (2004) 2681–2688.
[21] Z. Huang, X. Sun, Z. Xiu, S. Chen, C.T. Tsai, Precipitation synthesis and sintering of yttria nanopowders, Materials Letters 58 (2004) 2137–2142.
[22] J. Kong, J. Lu, K. Takaichi, T. Uematsu, K. Ueda, D.Y. Tang, D.Y. Shen, H. Yagi, T. Yanagitani, A.A. Kaminskii, Diode-pumped $Yb:Y_2O_3$ ceramic laser, Applied Physics Letters 82 (2003) 2556–2558.